*J. Fluid Mech.* (1971), *vol.* 48, *part* 1, *pp.* 183–208
*Printed in Great Britain*



# Statistical properties of velocity derivatives in a turbulent field

By FRANÇOIS N. FRENKIEL

Computation and Mathematics Department, Naval Ship Research and Development Center, Washington, D.C.

AND PHILIP S. KLEBANOFF

National Bureau of Standards, Washington, D.C.

(Received 3 August 1970 and in revised form 23 December 1970)

High-speed digital computing methods are applied to the study of the statistical behaviour of turbulent velocity derivatives in a nearly isotropic turbulent field downstream of a grid. Higher-order correlations of turbulent velocity gradients, up to the eighth order, are measured. Contrary to the case of *velocities*, the higher even-order correlations of *velocity gradients* more clearly evidence the departure from a two-dimensional Gaussian probability distribution. Using non-Gaussian probability distribution laws the relations between different odd- and even-order correlations are obtained and compared with the experimental measurements. The conditions of similarity and isotropy are evaluated for the small-scale structure as evidenced by the behaviour of the turbulent velocity gradients. The concept of intermittency of the small-scale structure is also discussed.

## 1. Introduction

Even the most simple case of homogeneous and isotropic turbulence still requires extensive research, both theoretical and experimental. The study of turbulence in shear flows, such as the flow over a flat plate, or the study of atmospheric turbulence, is considerably more complicated and a better understanding of the structure of turbulence under idealized conditions is a necessary requirement for further progress. It is with this point of view that a long-range research investigation into the statistical characteristics of turbulent fields has been undertaken to provide significant data which would be of importance in understanding their microstructure. The application of high-speed digital computing methods to the measurement of turbulence has made it possible to obtain data hitherto not readily available, and therefore, permits a more thorough exploration of experimental results and their theoretical consequences. Our previous studies of grid turbulence, using these techniques (Frenkiel & Klebanoff 1967*a*, *b*), have emphasized measurements of higher-order correlations of turbulent velocities and the degree to which these measurements are consistent with the assumptions of Gaussian probability density distribution and isotropy.

In the present paper the small-scale structure of the turbulence is investigated by applying a similar approach to the turbulent velocity gradients. In addition, an important aspect of the small-scale structure of turbulence is the question of intermittency. This question has been receiving more attention recently, both theoretical and experimental, particularly in connexion with the study of atmospheric and oceanographic turbulence. The presently unsettled situation in regard to the nature of intermittency, and the lack of an adequate evaluation of similarity for the small-scale structure, emphasize the need for further experimental investigation.

## 2. Experimental procedure

The present investigation was carried out in the nearly isotropic turbulence field generated by a square-mesh grid woven of iron rods, 0·5 cm in diameter, and a mesh, $M$, of 2·54 cm. The grid was placed perpendicular to the flow at the beginning of the test section of the 1·37 m wind tunnel at the National Bureau of Standards. The measurements presented were made at different distances, $X$, downstream of the grid, at 48·5 mesh-lengths and at 174·4 mesh-lengths, at a wind velocity, $U$, of approximately 15·2 m/sec. Measurements were also made at the 48·5 mesh-length position at a wind velocity of 7·6 m/sec. The intensity, $(\overline{u^2})^{\frac{1}{2}}/U$, of the longitudinal component of the turbulent velocity $u$, the Taylor microscale, $\lambda$, and the associated turbulence Reynolds number

$$R_\lambda = \frac{(\overline{u^2})^{\frac{1}{2}}\lambda}{\nu},$$

where $\nu$ is the kinematic viscosity corresponding to the foregoing experimental conditions, are given in table 1.

| $R_\lambda$ | $X/M$ | $U$ cm/s | $\dfrac{(\overline{u^2})^{\frac{1}{2}}}{U}$ | $\lambda/M$ ($M$ = 2·54 cm) |
|---|---|---|---|---|
| 37·7 | 48·5 | 759 | 0·0185 | 0·180 |
| 45·2 | 174·4 | 1564 | 0·00722 | 0·250 |
| 60·8 | 48·5 | 1518 | 0·0186 | 0·137 |

TABLE 1

Instrumentation combining analog and digital methods, similar to that described previously (Frenkiel & Klebanoff 1967*a*) was used. Constant-current hot-wire anemometry with compensated turbulence-measuring equipment was employed. The hot wires were platinum wires, 2·5 $\mu$ in diameter and 0·75 mm long. The fluctuating voltages corresponding to the longitudinal turbulent velocity, $u(t)$, and its first and second time derivatives, $du/dt$, $d^2u/dt^2$, were recorded simultaneously on magnetic tape, at a tape speed of 152·4 cm/sec using an Ampex CP–100 multichannel tape recorder. A timing signal of 12 800 Hz was simultaneously recorded on another channel. The analog tape was then digitized,

and the digital tapes were processed, using the computer facilities of the Computation and Mathematics Department, Naval Ship Research and Development Center. The analog data were digitized at a rate of 12 800 per second yielding samples of digitized data corresponding to analog recordings of approximately 12·5 seconds in duration. Digitizing was also carried out at the rate of 64 000 per second (with corresponding shorter sample lengths) in order to better define the correlation curves for small time delays. The time delay in the computer program was a multiple of the sampling rate. The results presented in this paper are based on four samples of recorded data at the highest Reynolds number listed in table 1 and on one sample of recorded data for each of the other two Reynolds numbers. In presenting the data for $R_\lambda = 60{\cdot}8$ the range of dispersion will be indicated wherever it is considered to be significant.

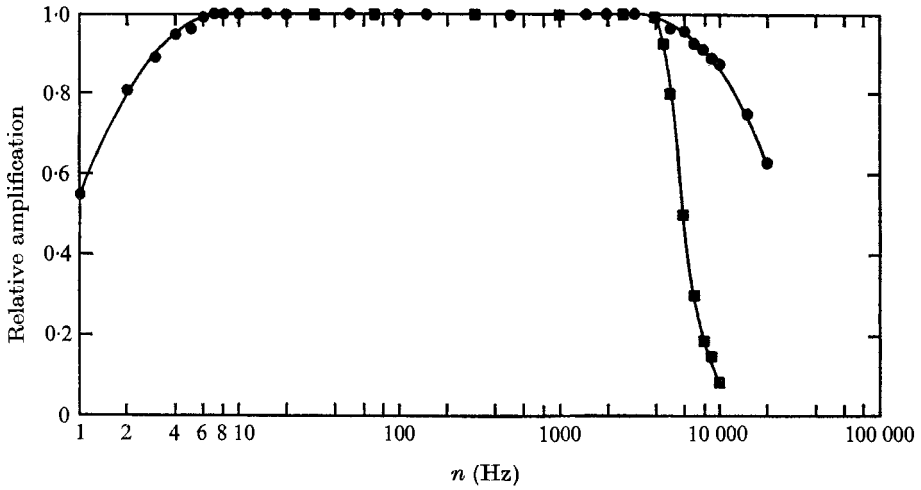


FIGURE 1. Frequency response. ●, $u$ channel; ■, $du/dt$ channel.

The differentiation was accomplished by using an operational amplifier in the differentiating mode which had adequate differentiating characteristics up to 10 000 Hz, i.e. the departure from linearity with frequency was 1 % at 10 000 Hz. The frequency response of the $u$ and $du/dt$ channels at the input to the tape recorder is shown in figure 1. The fall-off indicated in the relative amplification for the $du/dt$ channel represents the departure from a linear response with frequency. The more rapid fall-off, from the 1 % at 10 000 Hz noted above, is due to the characteristics of a Spencer–Kennedy low-pass electronic filter inserted in the $du/dt$ channel in order to improve the signal-to-noise characteristics. It should be noted that for the recording of the second derivative a similar differentiating operational amplifier, and a matching electronic filter set at the same cut-off frequency (5000 Hz) as for the first derivative were used. The data presented herein consist almost entirely of measurements involving the first derivative, and the signal-to-noise ratio for this quantity, including tape and digitizer noise, was 18 for the measurements made at the highest Reynolds number. This decreased to a signal-to-noise ratio of 11 at the lowest

Reynolds number. In this connexion, however, the frequency response illustrated in figure 1 remained the same at the different Reynolds numbers. No correction has been made to any of the data for the non-linear response of the hot wire, nor for noise. An estimate of the effect of the non-linear response of the hot wire on moments of the velocity derivatives up to the sixth-order was made and found not to be too significant within the experimental dispersion. A more precise evaluation of this non-linear effect, as well as an estimate of the effect on moments higher than the sixth will require measured correlations of higher order than presently available.

The selected frequency response, in particular as it relates to the measurement of derivatives, is always an important consideration, and at best represents a compromise between frequency response and the ratio of signal to noise. The adequacy of the frequency response in the present investigation can perhaps best be assessed from the measurements of the second moment of the spectral distribution shown in figure 2, where $F(n)$ is the normalized spectral function and $n$ is the frequency.

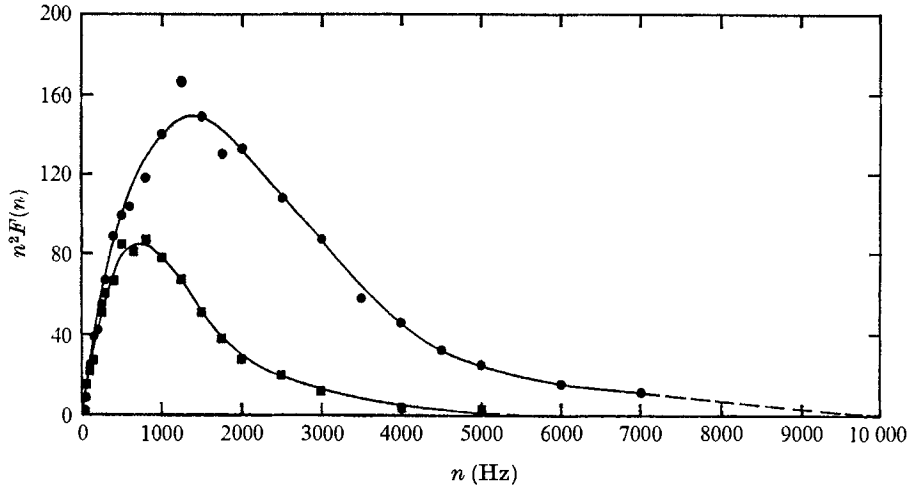


FIGURE 2. Second moment of spectral distributions.
●, $X/M = 48{\cdot}5$, $R_\lambda = 60{\cdot}8$; ■, $X/M = 174{\cdot}4$, $R_\lambda = 45{\cdot}2$.

The second moment of the spectral distribution is directly related to the mean-square turbulent velocity gradient in that

$$\frac{4\pi^2}{\overline{U}^2}\int_0^\infty n^2F(n)\,dn = \frac{1}{\lambda^2} \tag{1}$$

and

$$\frac{1}{\overline{U}^2\overline{u}^2}\overline{\left(\frac{du}{dt}\right)^2} = \frac{1}{\lambda^2}. \tag{2}$$

The values of $\lambda$ obtained using (1) for the distributions at $R_\lambda$ of 60·8 and $R_\lambda$ of 45·2 shown in figure 2 were 0·345 and 0·645 cm, respectively. In the case of the higher Reynolds number the distribution was arbitrarily closed as indicated by the dashed portion of the curve. These values of $\lambda$ agree very well with the values of

0·348 cm and 0·635 cm obtained directly from the digitized data using (2). It is, therefore, reasonable to conclude that the frequency response of the $du/dt$ channel was adequate, at least for the measurement of the time derivative at the two lower Reynolds numbers, and that no serious error was introduced at the higher Reynolds number. However, measurements of the second-order time derivative at the higher Reynolds number would be of questionable accuracy.

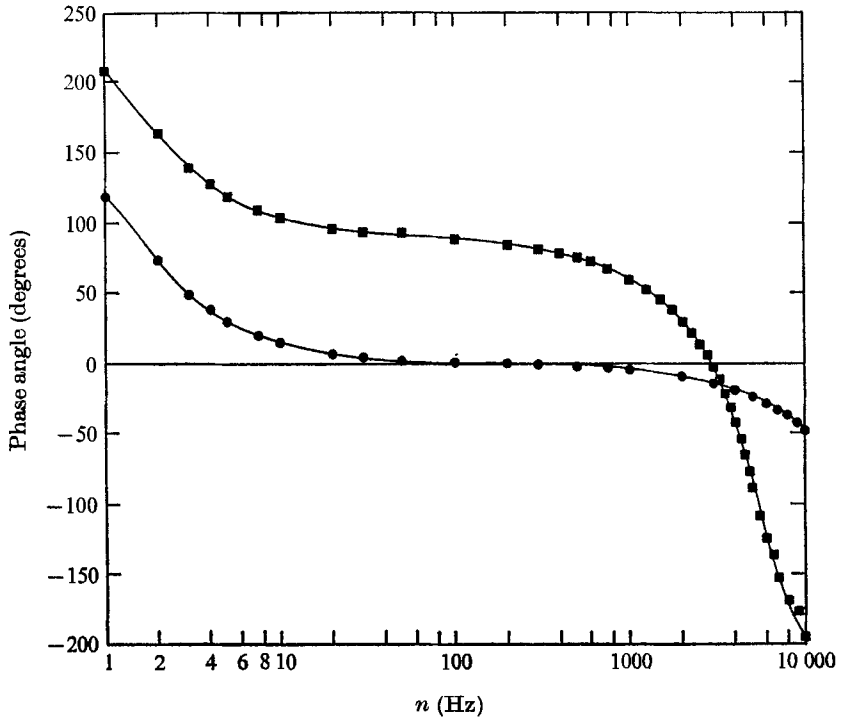


FIGURE 3. Phase shift as a function of frequency. ●, $u$ channel; ■, $du/dt$ channel.

In addition to the frequency response, another aspect requiring attention is that of the phase characteristics of the two channels. This is particularly important when measuring the time correlation of simultaneously recorded signals. The measured phase angles with frequency for the $u$ and $du/dt$ channels are shown in figure 3. A positive angle represents an advance in phase and a negative angle represents a lag in phase. The rapid variation of the phase angle with frequency for the $du/dt$ channel as compared with the $u$ channel is due to the low-pass filter. The frequency is plotted on a logarithmic scale; however, it should be noted that on a linear scale the phase angle for the $u$-channel is linear with frequency over most of the range, with increasing departure from linearity with decreasing frequency below 50 Hz. This departure is associated with the low frequency response of the a.c.-coupled hot-wire amplifier. On the other hand, the variation in phase with frequency for the $du/dt$ channel, due to the presence of the filter, does not remain linear over as great a range. It departs similarly at the lower frequencies but does not remain linear to as high a frequency as for the $u$ channel, departing

from linearity at about 4000 Hz. The aforementioned departure, at the lower frequencies, does not significantly affect the measurements of the correlations of derivatives since in such measurements the lower frequencies do not make a significant contribution. The differing phase characteristics of the $u$ and $du/dt$ channels introduce a small relative time delay between the two channels which, from the linear variation of phase with frequency for the respective channels referred to above, is estimated to be 69 $\mu$s. This time delay will be referred to again in connexion with the measurement of the time correlation of $u$ and $du/dt$ presented in § 4.

## 3. Probability distributions and intermittency

An important property attributed to the small-scale structure of turbulence at large turbulence Reynolds numbers is the intermittency of periods of activity and non-activity of a turbulent property such as velocity, velocity gradient, dissipation, etc. In the case of the velocity gradient, the degree of intermittency has been inferred from the magnitude of the fourth-order, $\overline{v_t^4}$, where

$$v_t = \frac{\partial u/\partial t}{[\overline{(\partial u/\partial t)^2}]^{\frac{1}{2}}}.$$

The existence of intermittency of the small-scale structure (at lower Reynolds numbers in the range of the present studies) was considered by Batchelor & Townsend (1949) with the tentative explanation that the intermittency is a manifestation of spatial spottiness of the small-scale structure. Evidence of similar spottiness within the inner region of the boundary layer (distinct from the well-known intermittency of the outer region) was demonstrated by Sandborn (1959). In evaluating the degree of intermittency from the flatness factor of the first derivative, $\overline{v_t^4}$, an intermittency factor $\gamma$ is defined as a fraction of the time (or space) during which the periods of activity exist. It is assumed that a turbulent property $p$ is zero during the periods of non-activity and that its statistical characteristics are unchanged during the several periods of activity. Thus,

$$\gamma \overline{p_{\text{turb}}^n} = \overline{p_{\text{int}}^n}, \tag{3}$$

where $p_{\text{turb}}$ is the property for the fully turbulent case ($\gamma = 1$) and $p_{\text{int}}$ corresponds to the intermittent condition ($\gamma < 1$). The above relation leads to

$$\left[\frac{\overline{p^n}}{\overline{(p^2)^{\frac{1}{2}n}}}\right]_{\text{int}} = \frac{1}{\gamma^{\frac{1}{2}n-1}} \left[\frac{\overline{p^n}}{\overline{(p^2)^{\frac{1}{2}n}}}\right]_{\text{turb}}. \tag{4}$$

If it is assumed that the probability density distribution of $p$ is Gaussian, then

$$\left[\frac{\overline{p^4}}{\overline{(p^2)^2}}\right]_{\text{turb}} = 3, \quad \left[\frac{\overline{p^6}}{\overline{(p^2)^3}}\right]_{\text{turb}} = 15, \quad \left[\frac{\overline{p^8}}{\overline{(p^2)^4}}\right]_{\text{turb}} = 105,$$

and, in general,

$$\left[\frac{\overline{p^{2n}}}{\overline{(p^2)^n}}\right]_{\text{turb}} = 1 \cdot 3 \cdot 5 \cdot \ldots (2n-1).$$

In particular for the velocity gradient $v_t(t)$

$$(\overline{v_t^4})_{\text{int}} = \frac{3}{\gamma}, \quad (\overline{v_t^6})_{\text{int}} = \frac{15}{\gamma^2}, \quad (\overline{v_t^8})_{\text{int}} = \frac{105}{\gamma^3}. \tag{5}$$

Table 2 gives the measured values of $\overline{v_t^n}$ for $n = 3$ to 8. Figure 4 presents the values of $\gamma$ obtained from the measured higher-order moments according to equations (5) for several values of the turbulence Reynolds number. The maximum and minimum deviations of the four samples for $R_\lambda = 60{\cdot}8$ are indicated in the figure.

| | $R_\lambda = 37{\cdot}7$ | $R_\lambda = 45{\cdot}2$ | $R_\lambda = 60{\cdot}8$ | Gaussian |
|---|---|---|---|---|
| $\overline{v_t^3}$ | 0·521 | 0·493 | 0·400 | 0 |
| $\overline{v_t^4}$ | 4·18 | 4·25 | 3·89 | 3 |
| $\overline{v_t^5}$ | 7·53 | 6·73 | 4·97 | 0 |
| $\overline{v_t^6}$ | 43·2 | 42·0 | 33·0 | 15 |
| $\overline{v_t^7}$ | 151 | 121 | 81·8 | 0 |
| $\overline{v_t^8}$ | 869 | 719 | 497 | 105 |

TABLE 2

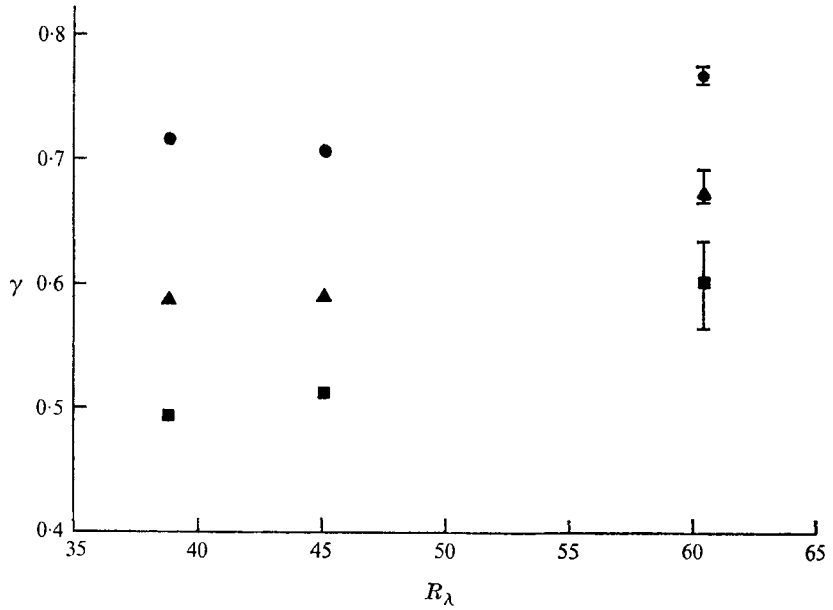


FIGURE 4. Intermittency factor $\gamma$ at several turbulence Reynolds numbers $R_\lambda$ as obtained from measured higher even-order moments. ●, $\gamma = 3/(\overline{v_t^4})_{\text{int}}$; ▲, $\gamma^2 = 15/(\overline{v_t^6})_{\text{int}}$; ■, $\gamma^3 = 105/(\overline{v_t^8})_{\text{int}}$.

In the case of an intermittency as described above, the values of $\gamma$ obtained from the different moments should be the same. However, this is not the case and we conclude that either the probability distribution cannot be considered as Gaussian, or the intermittency is of a different character from that we have assumed, or in fact, that there is no intermittency under the conditions corresponding to

figure 4. Nevertheless, intermittencies may still be observed with sufficient high-pass filtering although they are not observed for the over-all signals.

Figure 5 illustrates the nature of the fluctuating longitudinal turbulent velocity $u(t)$ and of its first and second time derivatives $\partial u/\partial t$ and $\partial^2 u/\partial t^2$ at a point located at 48·5 mesh-lengths downstream of a 2·54 cm square-mesh woven grid at a mean velocity of 15·18 m/sec. These data have been obtained from the analog tape recordings after digitizing at a rate corresponding to 64 000 per second. The magnitudes of the velocities and their derivatives are shown in figure 5 in arbitrary units. The recordings show no evidence of intermittency on the order of $\gamma$ from about 0·5 to 0·75 (as indicated by the data in figure 4) not only for the velocity gradient $\partial u/\partial t$ but even for the smaller-scale structure as indicated by $\partial^2 u/\partial t^2$.

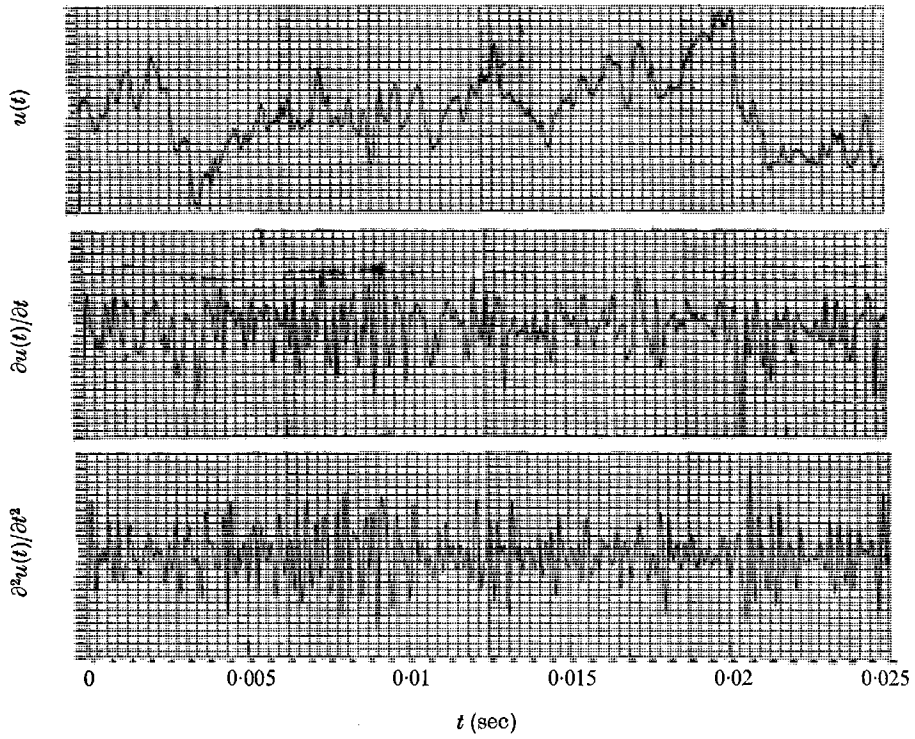


FIGURE 5. Recordings of the longitudinal turbulent velocity $u(t)$ and of its derivatives $\partial u/\partial t$ and $\partial^2 u/\partial t^2$ at the turbulence Reynolds number $R_\lambda = 60{\cdot}8$.

In view of the observed lack of intermittency in the present experiments in contrast to the measurements of Batchelor & Townsend, made under similar experimental conditions, we compare in figure 6 the actual values of $\overline{v_t^4}$ and its variation over a limited range of $R_\lambda$. The measurements presented in figure 6, obtained by different techniques (the present experiments by digital methods and the earlier results by analog procedures), are in good agreement and show little variation with Reynolds number. It should be noted that the cut-off frequency may affect measurements of this type. As discussed in § 2, it does not

appear likely, particularly at the lower $R_\lambda$, that this would have a significant effect on the present measurements. It should, however, be noted that there is a possibility that the effect of cut-off may be a source of error at the higher Reynolds numbers.

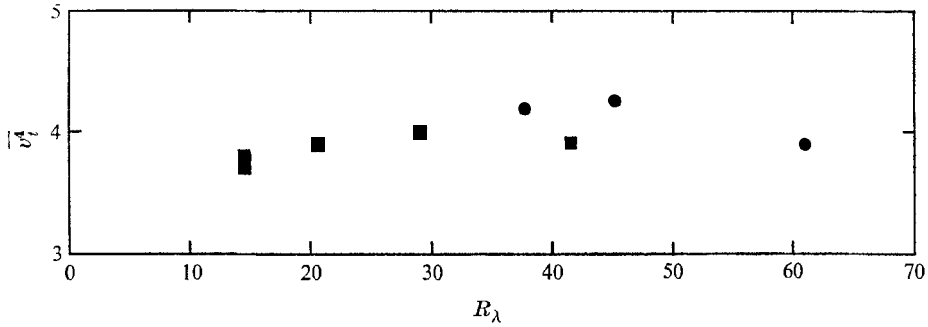


FIGURE 6. Flatness factors, $\overline{v_t^4}$, at several turbulence Reynolds numbers. ■, Batchelor–Townsend; ●, Frenkiel–Klebanoff.

To evaluate the smaller-scale structure even further, the flatness factor of the second derivative was measured at the lower Reynolds number ($R_\lambda = 37{\cdot}7$) to minimize the effect of the cut-off frequency, and the value of 5·3 was obtained which compares favourably with the value of 5·1 obtained by Batchelor & Townsend at a Reynolds number of 41·4. The difference between the measured $\overline{v_t^4}$ and that corresponding to a Gaussian distribution ($\overline{v_t^4} = 3$) can, therefore, be more appropriately attributed for the present experimental conditions, to the non-Gaussian character of the probability distribution of the velocity gradient rather than to intermittency of the type characterized by equation (3).

It is well known that the probability density distribution of the longitudinal turbulent velocities is very close to a Gaussian distribution (Frenkiel & Klebanoff 1965). On the other hand, as seen in figure 7, the measured probability density distribution of the velocity gradient $\mathscr{P}(v_t)$ departs from a Gaussian distribution. The measurements were made at 48·5 mesh-lengths downstream of the 2·54 cm mesh grid at a mean velocity of about 15·2 m/sec and a turbulence Reynolds number of about 61. The measured distribution represents an average over nine sample-distributions, each of approximately 12·5 seconds duration, sampled at a rate of 12800 per second. The nature of the departure from Gaussianity is better illustrated in figure 8 where the measured value of $v_t^3 \mathscr{P}(v_t)$ is presented as a function of $v_t$ and compared with a corresponding curve for a Gaussian distribution. It can now be readily seen (from figures 7 and 8) that the contribution to the skewness factor, $\overline{v_t^3}$, is due mainly to large positive values of $v_t$ although the small negative values of $v_t$ have a higher probability.† The value of the skewness factor of the derivatives obtained from the probability distribution

$$\overline{v_t^3} = \int_{-\infty}^{+\infty} v_t^3 \mathscr{P}(v_t)\, dv_t = 0{\cdot}410$$

† It should be noted that, if we assume the turbulent field to move like a frozen pattern with the mean velocity (Taylor's approximation) then $\partial u/\partial x = -(\partial u/\partial t)/U$ and thus the space-skewness factor has a sign opposite to that of the time-skewness factor.

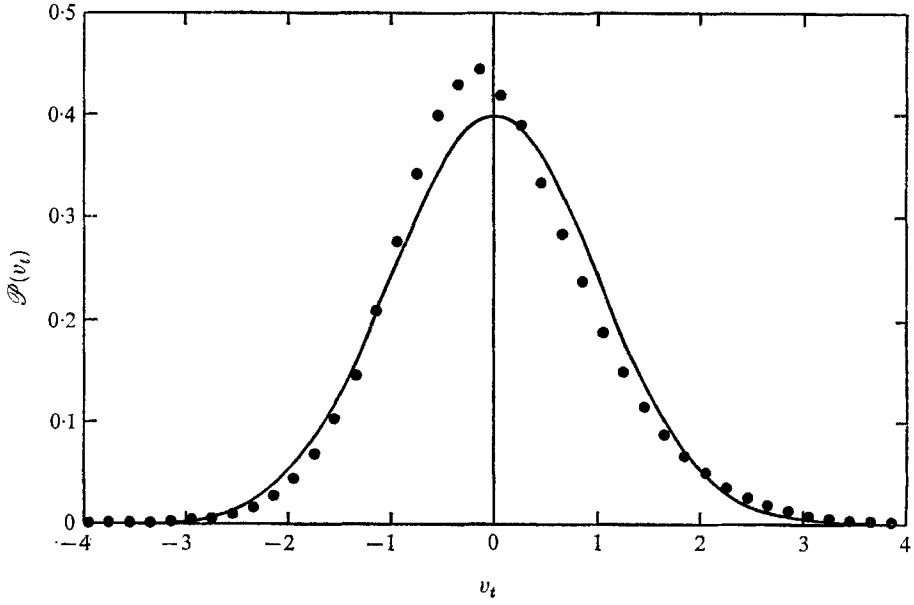


FIGURE 7. Comparison of the measured probability density distribution of the non-dimensional velocity gradient, $v_t$, with a Gaussian distribution. ●, measured; ——, Gaussian.

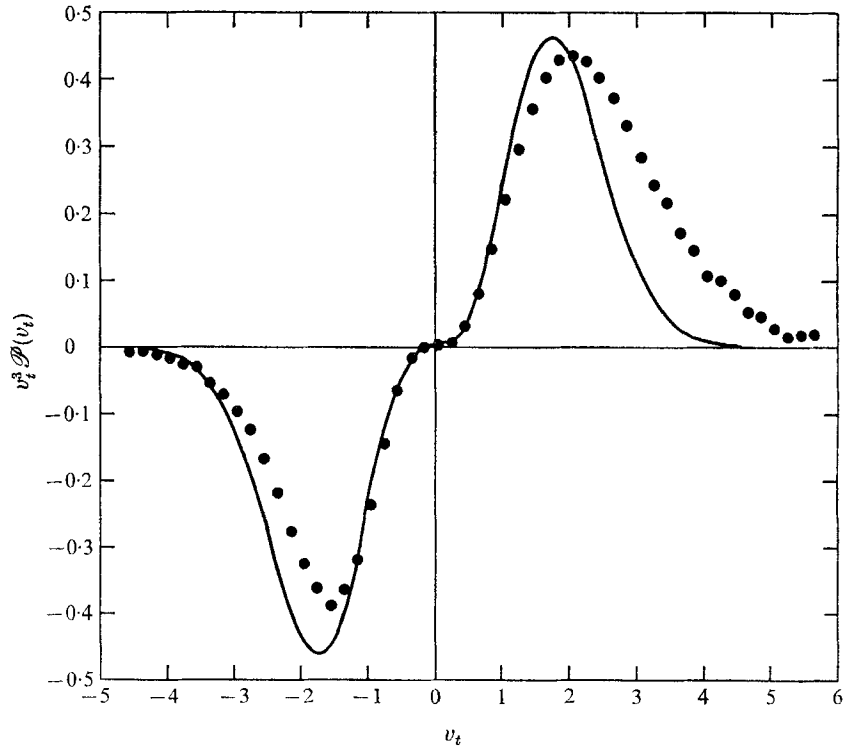


FIGURE 8. Comparison of the measured third moment of the probability density distribution of $v_t$ with the third moment of a Gaussian distribution. ●, measured; ——, Gaussian.

is in good agreement with the value $\overline{v_t^3} = 0{\cdot}409$ obtained directly from the digitized data.

The concept of intermittency of the small-scale structure of turbulence has led to the proposition, at higher Reynolds numbers, of a randomly intermittent dissipation field characterized by a log-normal probability distribution density for the dissipation (Kolmogoroff 1962, Obukhov 1962, Gurvich & Yaglom 1967). For the nearly isotropic turbulent field downstream of a grid, the dissipation is represented fairly well by the measured $\overline{v_t^2}$ when assuming the validity of the Taylor approximation. While the present experiments are made at much lower Reynolds numbers than those at which a log-normal distribution may be expected to apply, it is of interest to make this comparison in order to ascertain how well such a distribution approximates the measured data and to illustrate the intricacies of such a comparison.

The log-normal distribution for a property $\rho$ can be expressed as

$$P(\ln\rho) = \frac{1}{\sigma(2\pi)^{\frac{1}{2}}} \exp\left[-\frac{1}{2\sigma^2}(\ln\rho - \mu)^2\right],$$

with the related averages

$$\overline{\rho} = \exp(\mu + \tfrac{1}{2}\sigma^2) \quad \text{and} \quad \overline{\rho^2} = \exp(2\mu + 2\sigma^2)$$

and where the mean $\mu = \overline{\ln\rho}$ and the standard deviation $\sigma = [\overline{(\ln\rho - \mu)^2}]^{\frac{1}{2}}$.

In the present case, for $\rho = v_t^2$, we have

$$\overline{\rho} = \overline{v_t^2} = 1$$

and therefore,
$$\mu = -\tfrac{1}{2}\sigma^2 \tag{6}$$

and
$$\sigma^2 = \ln(\overline{\rho^2}) = \ln(\overline{v_t^4}). \tag{7}$$

Figure 9 presents a comparison between the measured cumulative probability density distribution of $\ln v_t^2$ (for the same data as presented in figure 7) and two log-normal distributions which in this figure are represented by straight lines. The log-normal distribution represented by the solid line was obtained by determining its mean $\mu$ and its standard deviation $\sigma$ from the measured flatness factor ($\overline{v_t^4} = 3{\cdot}975$) obtained directly from the nine samples of the digitized data using equations (6) and (7). The mean and the standard deviation for this distribution do not, however, correspond to the actual mean and standard deviation of the measured distribution of $\ln v_t^2$. The dashed line, on the other hand, represents a more appropriate log-normal distribution since it has the same $\mu$ and $\sigma$ as the measured distribution. A somewhat clearer comparison between the measured data and the log-normal distributions is given by presenting the probability densities $\mathscr{P}(\ln v_t^2)$ as functions of $\ln v_t^2$ in figure 10. These two figures clearly indicate that the log-normal distribution does not adequately characterize the measured results under present conditions.

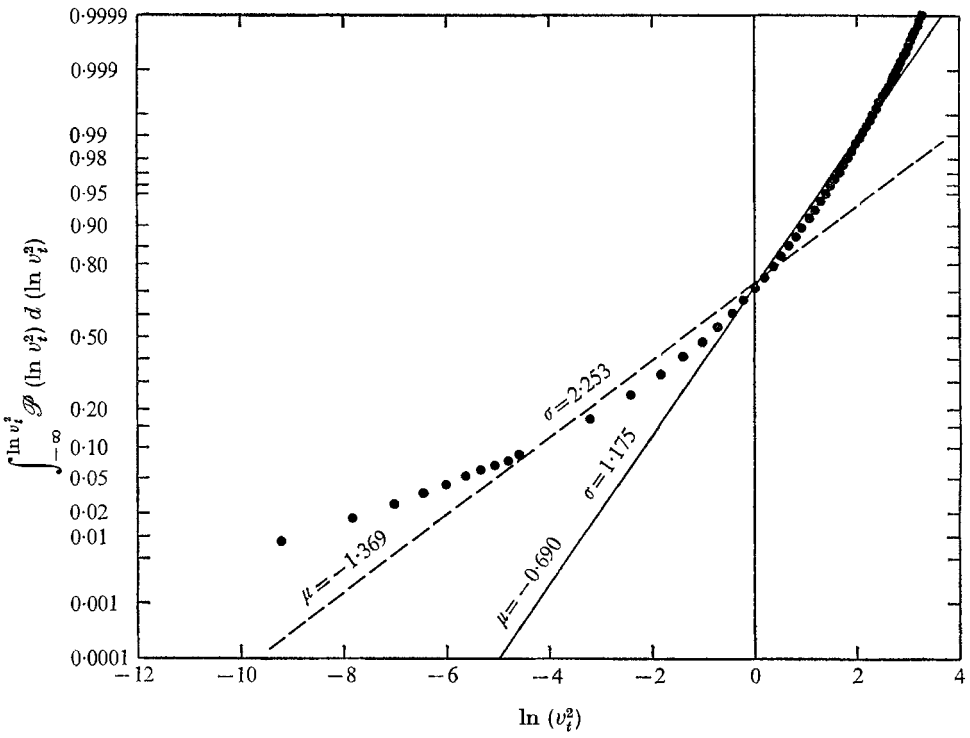


FIGURE 9. Comparison of the measured cumulative probability distribution of $\ln v_t^2$ with two log-normal distributions.

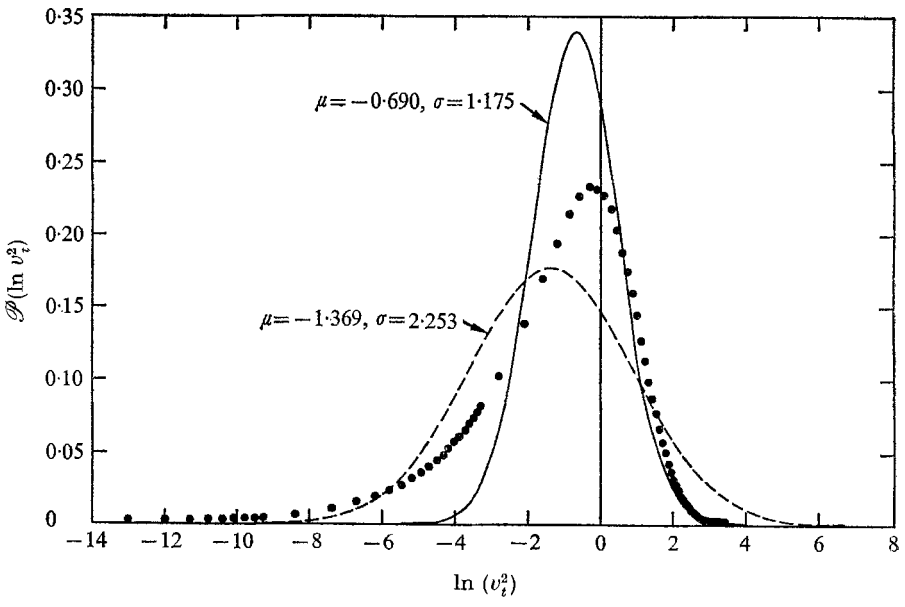


FIGURE 10. Probability density distributions corresponding to figure 9.

## 4. Correlations

The degree to which the probability distribution is Gaussian as well as the isotropy and similarity conditions for grid turbulence have received considerable attention. Most of the studies on this subject have been limited to the consideration of the character of the longitudinal turbulent velocity components and a larger scale structure. In the present paper an attempt is made to extend these studies to a smaller scale structure as reflected by the behaviour of the turbulent velocity gradient. In this connexion we shall refer to correlation of different orders of the derivatives of turbulent velocities.

$$T^{m,n}_{p,q}(h) = \frac{\overline{\left[\frac{\partial^p u(t)}{\partial t^p}\right]^m \left[\frac{\partial^q u(t+h)}{\partial t^q}\right]^n}}{\left[\overline{\left(\frac{\partial^p u(t)}{\partial t^p}\right)^2}\right]^{\frac{1}{2}m} \left[\overline{\left(\frac{\partial^q u(t+h)}{\partial t^q}\right)^2}\right]^{\frac{1}{2}n}}.$$

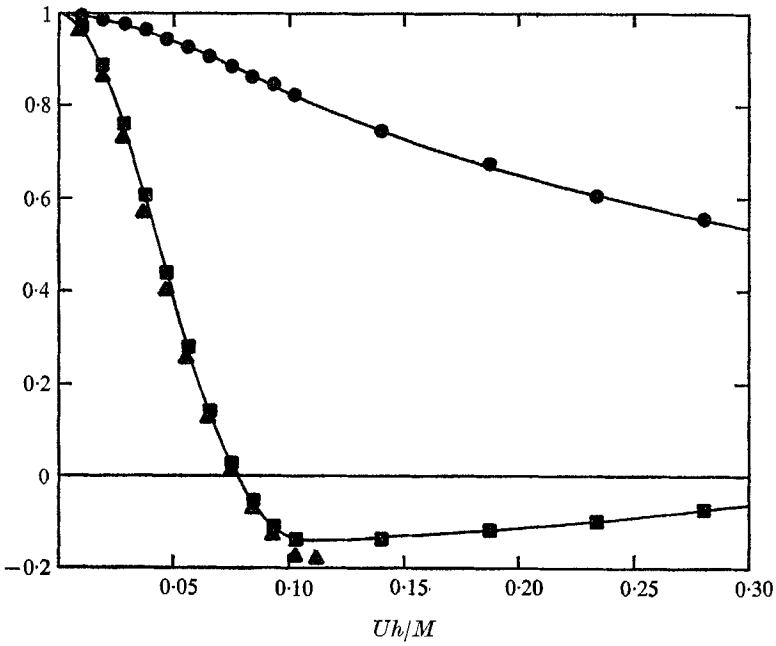


FIGURE 11. Comparison of the measured second-order correlation of turbulent velocities $R(h)$ with the second-order correlation of turbulent velocity gradients $T^{1,1}_{1,1}(h)$. ●, $R(h)$; ■, $T^{1,1}_{1,1}(h)$; ▲, $-\dfrac{\overline{u^2}}{\overline{(\partial u/\partial t)^2}}\dfrac{\partial^2 R(h)}{\partial h^2}$.

Figure 11 compares the measured second-order correlation of the turbulent velocity gradient

$$T^{1,1}_{1,1}(h) = \frac{\overline{v_t(t)\, v_t(t+h)}}{\overline{v_t^2}}$$

with the second-order correlation of the turbulent velocity

$$R(h) = T^{1,1}_{0,0}(h) = \frac{\overline{u(t)\, u(t+h)}}{\overline{u^2}}$$

as functions of the time interval $h$. The data presented in the figure were obtained at 48·5 mesh-lengths downstream of the grid and at a mean wind velocity of 15·18 m/sec. The comparison exhibits the markedly different behaviour of the two correlation curves. In contrast to the correlation curve for the turbulent velocities, the integral of the correlation curve for the turbulent velocity gradients cannot be used to characterize a scale of turbulence since this integral should be

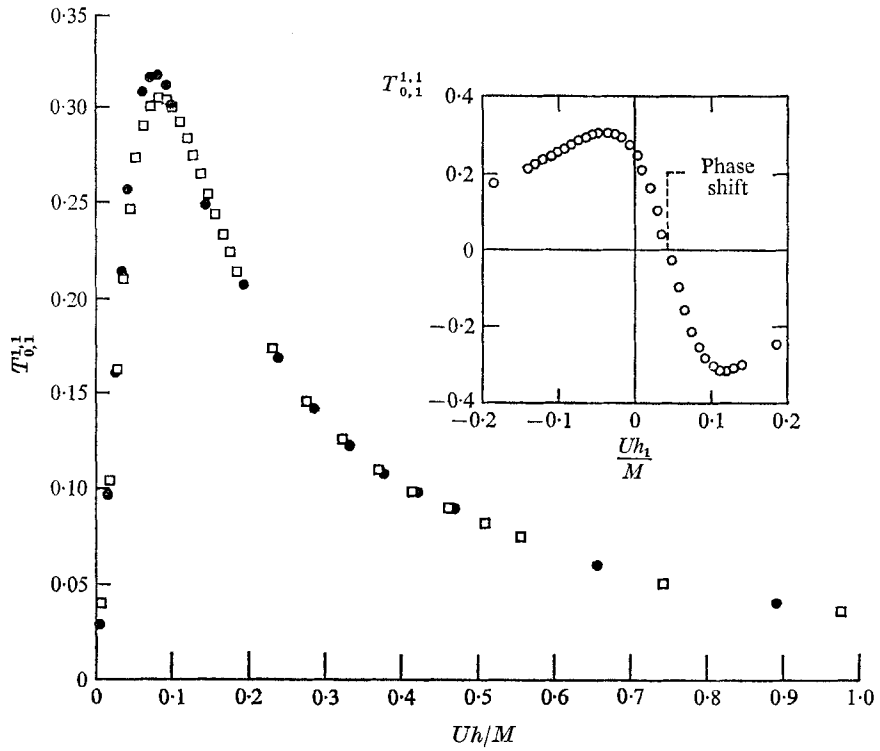


FIGURE 12. Second-order correlation between the turbulent velocity and its gradient. □, $T^{1,1}_{0,1}(-h)$; ●, $-T^{1,1}_{0,1}(h)$.

equal to zero. In fact the curve illustrates this behaviour. Figure 11 also includes a comparison between the correlation $T^{1,1}_{1,1}(h)$ measured directly and its value obtained by numerical differentiation of the correlation $R(h)$ according to the relations

$$\frac{\partial^2 R(h)}{\partial h^2} = -\frac{\partial^2}{\partial t^2}\left[\frac{\overline{u(t)\,u(t+h)}}{\overline{u^2}}\right] = -\frac{1}{\overline{u^2}}\,\overline{\frac{\partial u(t)}{\partial t}\,\frac{\partial u(t+h)}{\partial t}}$$

$$T^{1,1}_{1,1}(h) = \frac{\partial^2 R(h)}{\partial h^2}\Big/\frac{\partial^2 R(0)}{\partial h^2} = -\frac{\overline{u^2}}{\overline{(\partial u/\partial t)^2}}\,\frac{\partial^2 R(h)}{\partial h^2}. \tag{8}$$

Although the accuracy of a double differentiation is not too satisfactory, the agreement between the two methods provides a fairly good check of the data. In performing the numerical differentiation the use of the data obtained with the higher sampling rate was required.

Figure 12 shows the measured second-order correlation between the turbulent velocity and its gradient

$$T^{1,1}_{0,1}(h) = \frac{\overline{u(t)\,\partial u(t+h)/\partial t}}{(\overline{u^2})^{\frac{1}{2}}\,[\overline{(\partial u/\partial t)^2}]^{\frac{1}{2}}}$$

for the same experimental flow conditions as for the results given in figure 11. An important consideration in such measurements is the relative phase shift between the two recorded signals (in the present case between $\partial u/\partial t$ and the $u$ channels). The insert in figure 12 presents the data as measured before taking into account the phase shift. In this insert $T^{1,1}_{0,1}$ is presented as a function of $Uh_1/M$, where $h_1 = h+\varphi$ with $\varphi$ representing the relative phase shift. For a stationary field of turbulence a necessary condition is

$$\overline{u(t)\,\partial u/\partial t(t)} = 0 \quad \text{or} \quad T^{1,1}_{0,1}(0) = 0.$$

Under such a condition the measured value of $h_1$ corresponding to $T^{1,1}_{0,1} = 0$ should give the relative phase shift $\varphi$. The phase shift, $\varphi$, obtained in this manner is 71 $\mu$s (corresponding to $Uh_1/M = 0{\cdot}0425$), which is in good agreement with the value of 69 $\mu$s estimated from direct measurements of the phase characteristics referred to in § 2. It is thus reasonable to consider the turbulent field for the present purposes as being stationary; however, a more thorough analysis of this question would require more extensive studies.

If we assume the Taylor approximation to be valid and that the turbulent field is isotropic, then the correlation curve $T^{1,1}_{0,1}(h)$ should be antisymmetric:

$$T^{1,1}_{0,1}(h) = -T^{1,1}_{0,1}(-h). \tag{9}$$

A comparison between the values of $T^{1,1}_{0,1}(h)$ and $T^{1,1}_{0,1}(-h)$ is made in figure 12 after taking into account the phase shift obtained from the measured correlations. This comparison indicates that the isotropic condition (9) is well satisfied. It should be noted that under the same experimental conditions the third-order correlations of the longitudinal turbulent velocity fluctuation did not exhibit the necessary antisymmetric condition (Frenkiel & Klebanoff 1967*b*), indicating that the larger scale structure is non-isotropic. However, it should also be noted that under similar conditions Van Atta & Chen (1968) found that the third-order correlations do satisfy the antisymmetric isotropy condition fairly well. Van Atta & Chen attribute the difference in their measurements of the third-order correlations of velocities, as compared to the present authors, to the differences in the low frequency response of the measuring equipment. It should be noted that it is not reasonable to expect that the measurements exhibit a greater degree of non-isotropy by eliminating the lower frequency fluctuations which for grid turbulence are non-isotropic. An estimate was also made by appropriate numerical methods of the correction for the response in amplitude and phase shift at lower frequencies and no significant effect was observed. In this connexion, Helland & Stegen (1970) have shown that the difference in the low frequency response of the measuring equipment is not the correct explanation for the observed differences in the third-order correlations.

While there is no reason why the decaying field of turbulence should be isotropic, there may still be some question as to the degree of non-isotropy. In this

context we shall examine the degree of isotropy of the smaller scale structure in greater detail as evidenced by the correlations $T_{1,1}^{m,n}(h)$ and $T_{1,1}^{n,m}(h)$ which should be equal in an isotropic field of turbulence. In figures 13 and 14 such a comparison is made for $m+n = 3$ and 5, respectively, for the three different experimental conditions listed in table 1. The maximum and minimum deviations for the four samples at the highest Reynolds number are not shown in these figures inasmuch as the individual samples exhibited the same degree of comparability

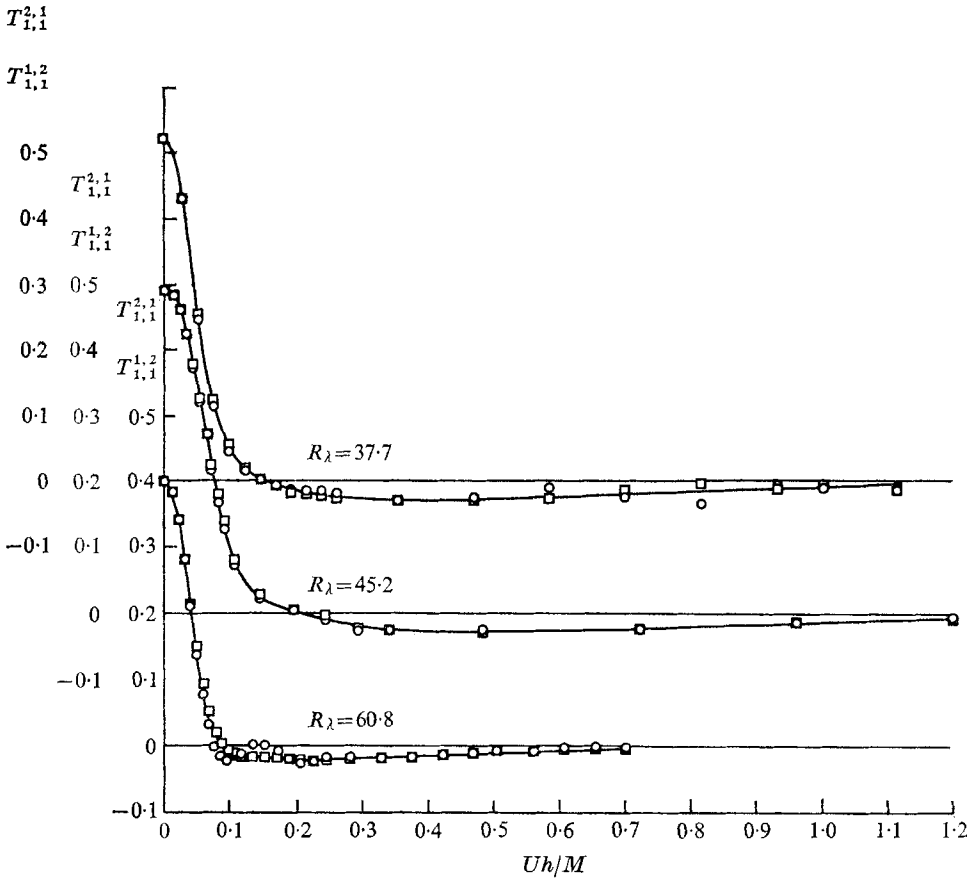


FIGURE 13. Third-order correlations of turbulent velocity gradients $T_{1,1}^{2,1}(h)$ and $T_{1,1}^{1,2}(h)$ for three Reynolds numbers. ○, $T_{1,1}^{2,1}$; □, $T_{1,1}^{1,2}$.

as the averages which are given in the figures. The differences between the correlations $T_{1,1}^{2,1}$ and $T_{1,1}^{3,2}$ as compared to the correlations $T_{1,1}^{1,2}$ and $T_{1,1}^{3,2}$, respectively, are rather small and there is no reason at present to consider them as being significant. We should, however, note that the relatively larger deviation of $T_{1,1}^{2,1}$ at $Uh/M = 0{\cdot}140$ for $R_\lambda = 60{\cdot}8$ was consistently observed. Figures 13 and 14 show that the moments $\overline{v_t^3} = T_{1,1}^{2,1}(0) = T_{1,1}^{1,2}(0)$ and $\overline{v_t^5}(0) = T_{1,1}^{3,2}(0) = T_{1,1}^{2,3}(0)$ are decreasing with increasing Reynolds number. In figure 15 the values of $\overline{v_t^3}$ are compared with those obtained by Batchelor & Townsend (1947). Their values are somewhat lower and also indicate a decrease with increasing $R_\lambda$.

Assuming the Taylor approximation, equation (8) can be rewritten as

$$T^{1,1}_{1,1}(h) = -\frac{\lambda^2}{U^2}\frac{\partial^2 R(h)}{\partial h^2}.$$

Similarity for the correlation curve as a function of $Uh/\lambda$ gives the relation

$$T^{1,1}_{1,1}(Uh/\lambda) = -\frac{\partial^2 R(Uh/\lambda)}{[\partial(Uh/\lambda)]^2}, \tag{10}$$

thus showing that, with $\lambda$ as a characteristic length-scale, similarity of the velocity-gradient correlations $T^{1,1}_{1,1}(Uh/\lambda)$ requires similarity of the velocity correlations $R(Uh/\lambda)$. Figure 16 shows the correlations $R(Uh/\lambda)$ and $T^{1,1}_{1,1}(Uh/\lambda)$ for

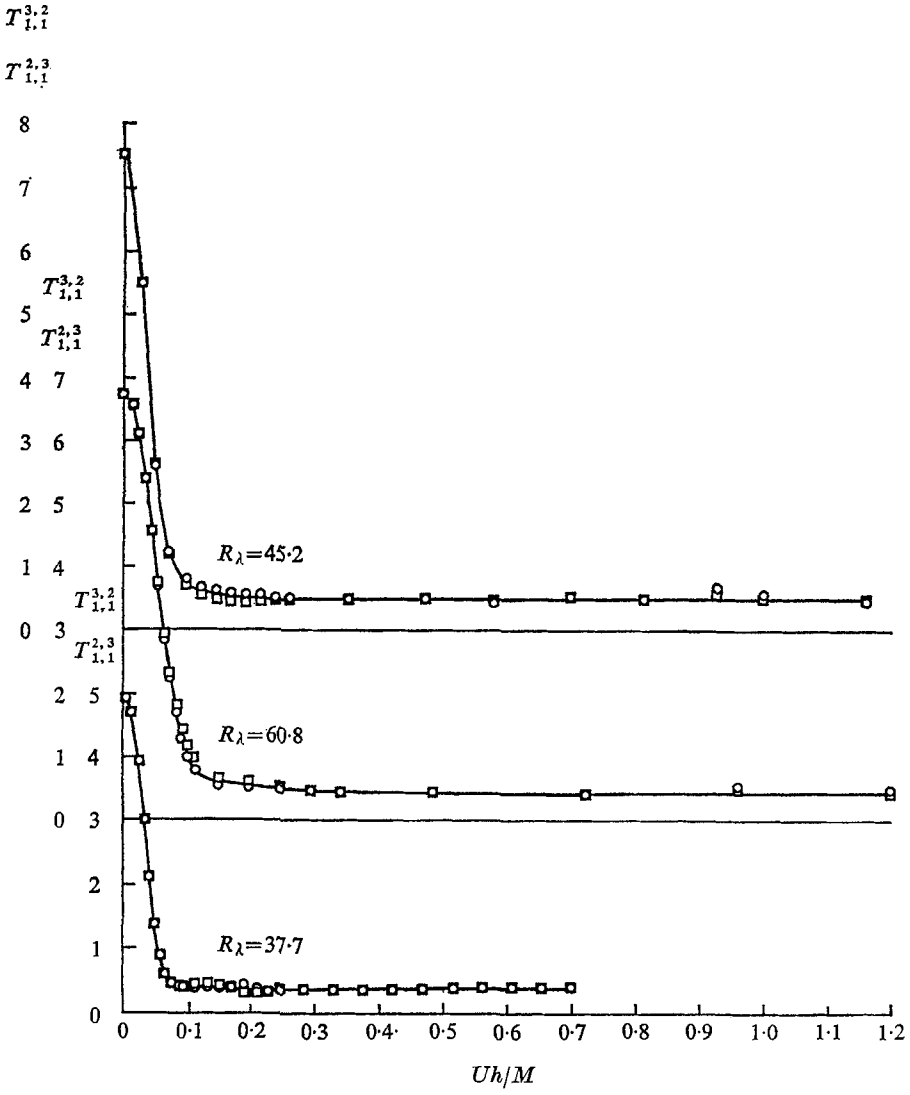


FIGURE 14. Fifth-order correlations $T^{3,2}_{1,1}(h)$ and $T^{2,3}_{1,1}(h)$ for three Reynolds numbers. ○, $T^{3,2}_{1,1}$; □, $T^{2,3}_{1,1}$.

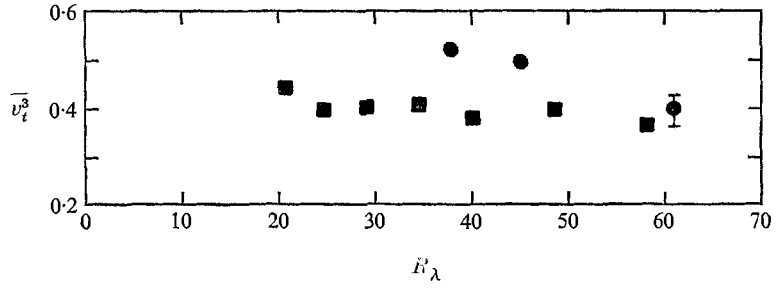


FIGURE 15. Skewness factors, $\overline{v_t^3}$, at several turbulence Reynolds numbers. ■, Batchelor–Townsend; ●, Frenkiel–Klebanoff.

the different Reynolds numbers $R_\lambda$. The velocity-correlations appear to be similar only for the relatively smaller scale structure as evidenced by their values for $Uh/\lambda$ smaller than 1. It should be noted that the value of $R_\lambda$ is not necessarily the determining parameter since the effect of the decay is also involved. Similar behaviour for the velocity correlations has also been observed by Stewart & Townsend (1951) at an approximately constant Reynolds number at different stages of decay. However, the velocity-gradient correlations $T^{1,1}_{1,1}$ exhibit a somewhat greater lack of similarity for the smaller scale structure.

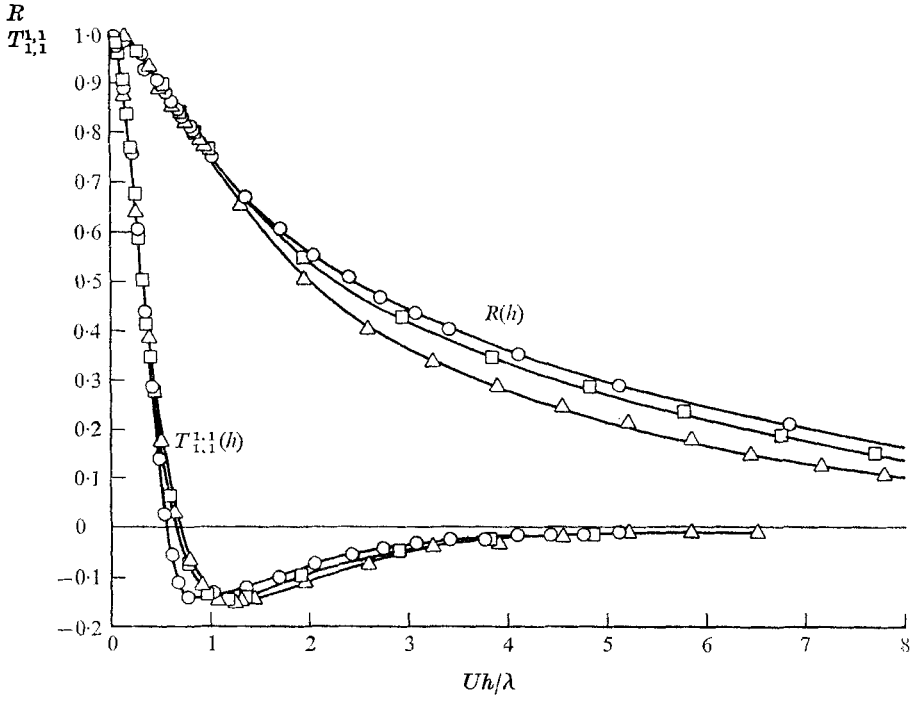


FIGURE 16. Evaluation of similarity of second-order correlations of turbulent velocities $R(h)$ and of turbulent velocity gradients $T^{1,1}_{1,1}(h)$, with microscale $\lambda$, for different Reynolds numbers $R_\lambda$: △, 37·7; □, 45·2; ○, 60·8.

It is also of interest to consider the similarity for the correlation curves $T^{1,1}_{1,1}(Uh/\eta)$ where $\eta$ is the Kolmogoroff length $(\nu^3/\epsilon)^{\frac{1}{4}}$ and $\epsilon$ is the rate of dissipation per unit mass. This gives the relation

$$T^{1,1}_{1,1}(Uh/\eta) = -\frac{\lambda^2}{\eta^2}\frac{\partial^2 R(Uh/\eta)}{[\partial(Uh/\eta)]^2} \tag{11}$$

and, with the isotropic relation for the rate of dissipation, one obtains

$$\eta = (15)^{-\frac{1}{4}}\frac{\lambda}{R_\lambda^{\frac{1}{2}}}.$$

It is thus seen that the restriction that similarity be satisfied for both velocity correlations and velocity-gradient correlations is not applicable with the Kolmogoroff length as the characteristic scale as long as $\eta/\lambda$ is not constant.

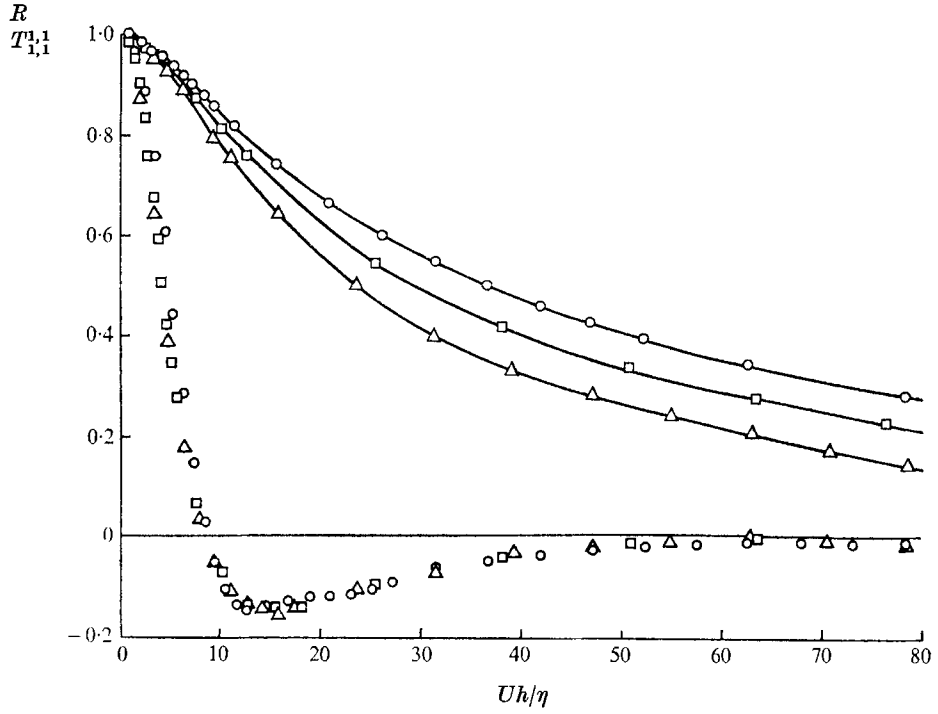


FIGURE 17. Evaluation of similarity of second-order correlations $R(h)$ and $T^{1,1}_{1,1}(h)$, with Kolmogoroff scale $\eta$, for different Reynolds numbers. See figure 16 for symbols.

Figure 17 presents the two correlation curves $R$ and $T^{1,1}_{1,1}$ as functions of $Uh/\eta$ at the three Reynolds numbers. As expected the velocity correlations are more dissimilar with $\eta$ as a length-scale than with $\lambda$, but on the other hand, the velocity gradient correlations exhibit a greater degree of similarity. Within the experimental uncertainty it is difficult to evaluate the small departures from a single curve at small values of $Uh/\eta$.

Figure 18 presents the third-order correlations $T^{2,1}_{1,1}$ and $T^{1,2}_{1,1}$ as functions of $Uh/\eta$ at the three Reynolds numbers, and figure 19 presents a similar plot for the fourth-order correlation $T^{2,2}_{1,1}$. These last two figures also indicate a considerable

degree of similarity particularly for the larger values of $Uh/\eta$. It is interesting to note that if there is a variation of the third- and fourth-order moments

$$T^{2,1}_{1,1}(0) = T^{1,2}_{1,1}(0) = \overline{v_t^3} \quad \text{and} \quad T^{2,2}_{1,1}(0) = \overline{v_t^4}$$

with Reynolds number, then the similarity at very small $Uh/\eta$ cannot be expected. Thus, any model of a small-scale intermittency which results in the variation of such moments with the Reynolds number cannot be fully consistent with the similarity condition, and therefore the curves in figure 18 are not extended to the origin.

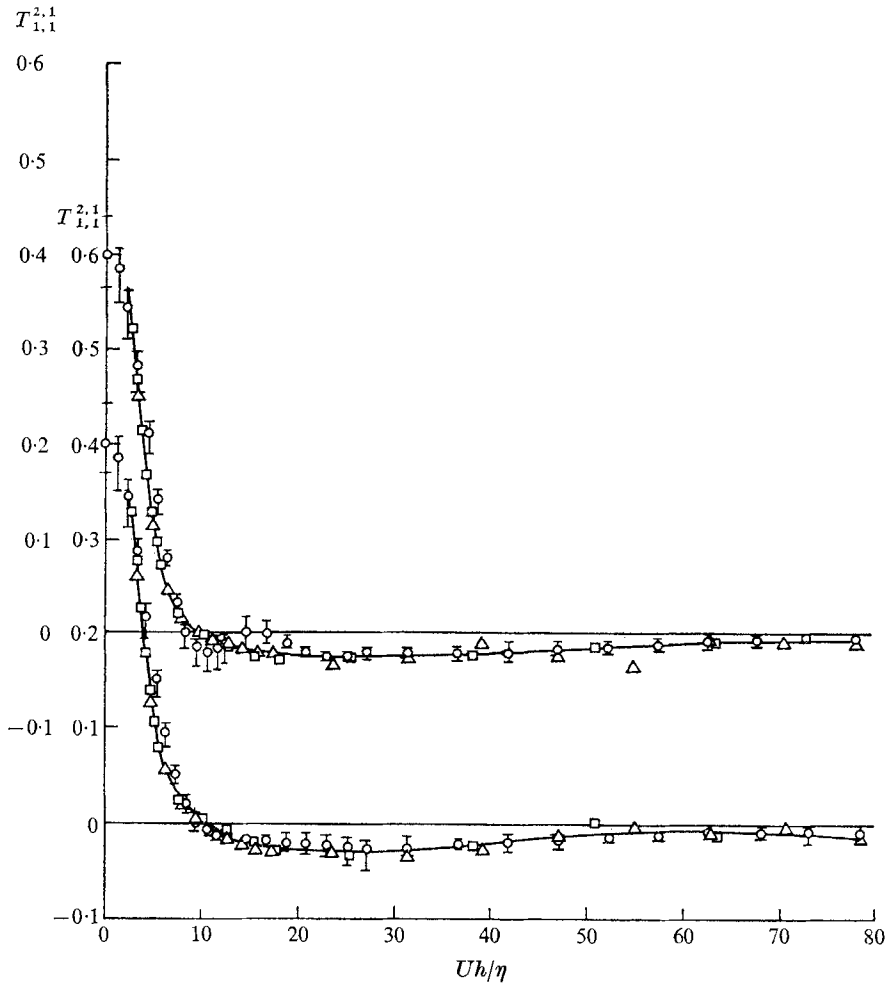


FIGURE 18. Evaluation of similarity of third-order correlations $T^{2,1}_{1,1}(h)$ and $T^{1,2}_{1,1}(h)$ with $\eta$. See figure 16 for symbols.

It is also of interest to examine the similarity of the two dissipation spectra shown previously in figure 2. These spectral data, with the non-normalized spectral function $\phi(\kappa) = \overline{u^2}F(\kappa)$ and $\kappa = 2\pi n/U$ are replotted in figure 20 with $\eta$ and $v$ as effective scales, where $v$ is the Kolmogoroff velocity $(\nu\epsilon)^{\frac{1}{4}}$. This representation

gives a constant area under the curves which for an isotropic turbulence would be equal to 1/15 and in the case of similarity would yield a single curve over the whole range of $\kappa$ values. It is seen that there is some departure from this condition and it appears that the spectrum may provide a more sensitive criterion for similarity than the correlation.

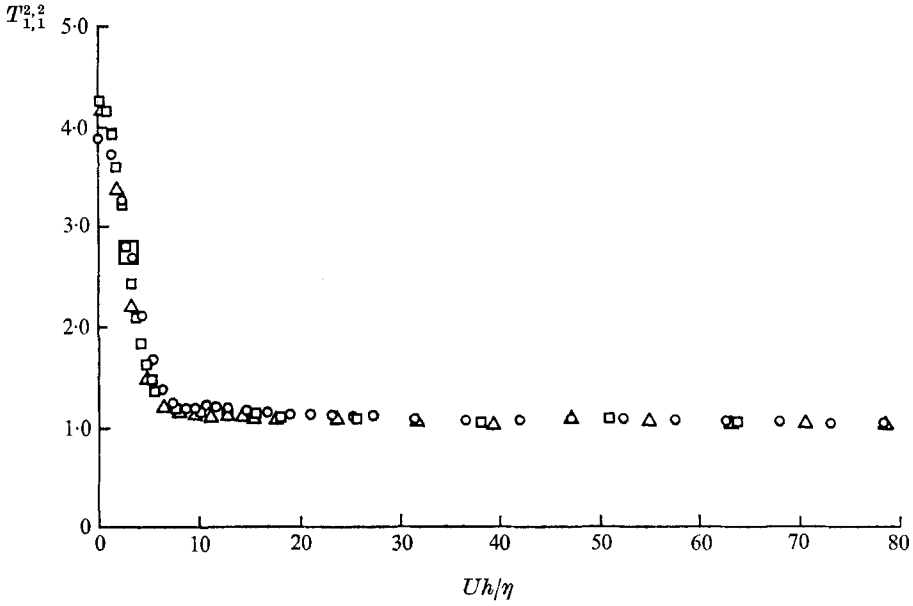


FIGURE 19. Evaluation of similarity of the fourth-order correlation $T^{2,2}_{1,1}(h)$ with $\eta$. See figure 16 for symbols.

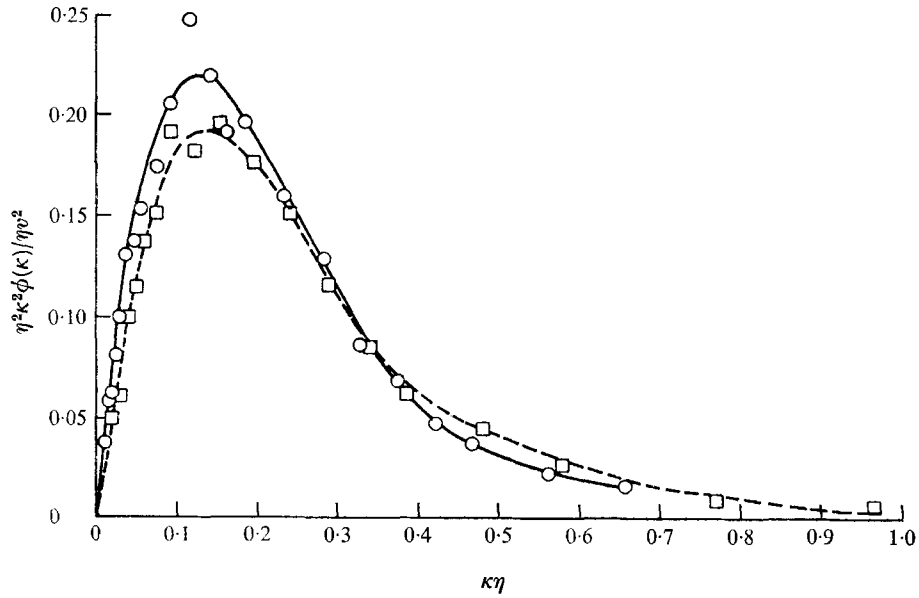


FIGURE 20. Evaluation of similarity of dissipation spectra with $\eta$ for two Reynolds numbers. – – □ – –, $R_\lambda = 45{\cdot}2$; —○—, $R_\lambda = 60{\cdot}8$.

The non-Gaussian nature of the probability density distribution of the turbulent velocity gradient has been discussed in § 3. We shall now consider the degree to which the correlations reflect this non-Gaussianity.

If we assume that the two-dimensional probability distribution of the velocity-gradient is Gaussian, then the fourth-order correlations are related to the second-order correlations by the expressions

$$T^{3,1}_{1,1} = T^{1,3}_{1,1} = 3T^{1,1}_{1,1} \quad \text{and} \quad T^{2,2}_{1,1} = 1 + 2(T^{1,1}_{1,1})^2. \tag{12}$$

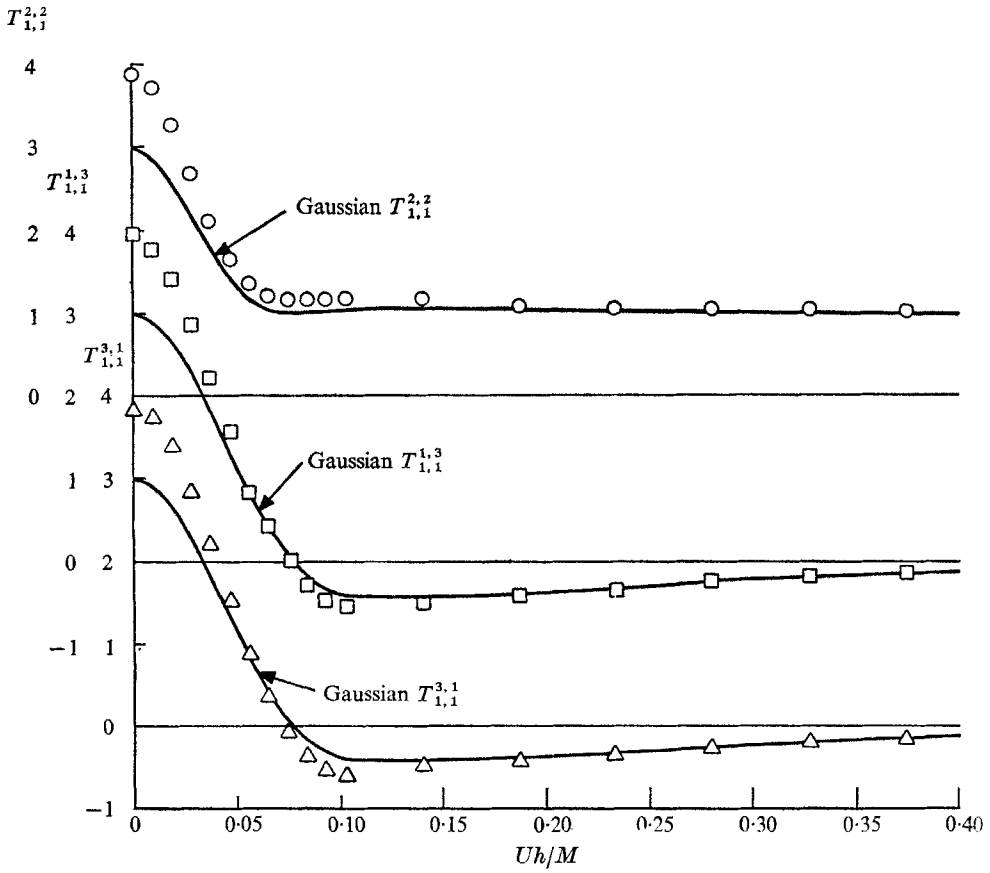


FIGURE 21. Comparison of the measured fourth-order correlations $T^{2,2}_{1,1}(h)$, at $R_\lambda = 60{\cdot}8$, with the correlation obtained for a Gaussian distribution of turbulent velocity gradients $v_t$.

In figure 21 we compare the measured fourth-order correlations for $R_\lambda = 60{\cdot}8$ with those obtained from equations (12). The disagreement is in marked contrast to a similar comparison of turbulent velocities (Frenkiel & Klebanoff 1967*a*). It may be noted that the measured values of $T^{3,1}_{1,1}$ and $T^{1,3}_{1,1}$ are in close agreement in support of the isotropy condition referred to previously. Let us now examine the non-Gaussianity by assuming that the two-dimensional probability density distribution is of the Gram-Charlier type according to the equation

$$\mathscr{P}(v_t(t), v_t(t+h)) = \mathscr{P}_0(v_t(t),\ v_t(t+h)) \sum_0^{j+k} A_{j,k} H_{j,k}(v_t(t), v_t(t+h)), \tag{13}$$

where $\mathscr{P}_0$ is the Gaussian distribution

$$\mathscr{P}_0(v_t(t), v_t(t+h)) = \frac{1}{2\pi[1-(T^{1,1}_{1,1})^2]^{\frac{1}{2}}} \exp\left\{-\frac{1}{2[1-(T^{1,1}_{1,1})^2]} \times \{[v_t(t)]^2 - 2T^{1,1}_{1,1} v_t(t)\, v_t(t+h) + [v_t(t+h)]^2\}\right\}$$

and where $H_{j,k}$ is a Hermite polynomial of two variables and $A_{j,k}$ are coefficients which can be defined in terms of the higher-order correlations $T^{m,n}_{1,1}$ (Kampé de Fériet 1966; Frenkiel & Klebanoff 1967*a*). Considering now the fourth-order non-Gaussian probability distribution (13) with $j+k=4$, we find such correlations as

$$T^{3,2}_{1,1} = \overline{v_t^3} + 6T^{1,1}_{1,1}T^{2,1}_{1,1} + 3T^{1,2}_{1,1}, \tag{14}$$

$$T^{3,3}_{1,1} = 3T^{3,1}_{1,1} + 9T^{1,1}_{1,1}T^{2,2}_{1,1} + 3T^{1,3}_{1,1} - 12(T^{1,1}_{1,1})^3 - 18T^{1,1}_{1,1}, \tag{15}$$

$$T^{4,3}_{1,1} = 3\overline{v_t^3}(4T^{1,1}_{1,1} + 1) + 18[1 + 2(T^{1,1}_{1,1})^2]\, T^{2,1}_{1,1} + 36T^{1,1}_{1,1}T^{1,2}_{1,1}, \tag{16}$$

$$T^{4,4}_{1,1} = 6\overline{v_t^4} + 48T^{1,1}_{1,1}(T^{3,1}_{1,1} + T^{1,3}_{1,1}) + 36[1 + 2(T^{1,1}_{1,1})^2]\, T^{2,2}_{1,1} - 120(T^{1,1}_{1,1})^4 - 360\,(T^{1,1}_{1,1})^2 - 45. \tag{17}$$

The above correlations are expressed in terms of measured lower-order correlations, meaning measured correlations for $m+n = 2, 3$ and 4.

Figure 22 compares the measured fifth-order correlation $T^{3,2}_{1,1}$, for $R_\lambda = 60{\cdot}8$, with the corresponding correlation obtained according to equation (14). The open circles denote the average values of four samples with a range of deviation as indicated. The correlation curve corresponding to the fourth-order non-Gaussian distribution has been computed using the average values of the lower-order correlations. In the case of a Gaussian probability distribution these correlations (like all other odd-order correlations) would be zero. The fourth-order non-Gaussian distribution thus results in a much better approximation to the measured correlations with fairly good agreement for values of $Uh/M > 0{\cdot}04$. The departure of the measured correlations from those obtained according to (14) for $Uh/M < 0{\cdot}04$ is reflected in the ratio of the moments $\overline{v_t^5}/\overline{v_t^3}$, which in the case of the fourth-order non-Gaussian distribution should be 10 as compared to the measured ratio of about 12·5 (as seen from table 2) for $R_\lambda = 60{\cdot}8$.

A similar comparison is made in figure 23 for the sixth-order correlation $T^{3,3}_{1,1}$. The measured correlation is compared with the correlation corresponding to a Gaussian distribution

$$T^{3,3}_{1,1} = 3T^{1,1}_{1,1}[3 + 2(T^{1,1}_{1,1})^2] \tag{18}$$

as well as with that corresponding to the fourth-order non-Gaussian distribution given by equation (15). Comparison of the measured $T^{3,3}_{1,1}$ with that obtained for the fourth-order non-Gaussian distribution exhibits a behaviour similar to $T^{3,2}_{1,1}$ with somewhat closer agreement at the small values of $Uh/M$.

We may note that the data presented in figures 22–23 were obtained using digitizing rates of 64 000 per second with sample lengths of approximately 2·5 seconds. The maximum and minimum deviations in values of correlation obtained from four different samples of data are indicated in the figures. Similar

data (not presented here) were obtained with digitizing rates of 12 800 per second and sample lengths of about 12·5 seconds. However, the deviations, from sample to sample, obtained with the slower digitizing rates were essentially of the same order, and the average values were approximately the same.

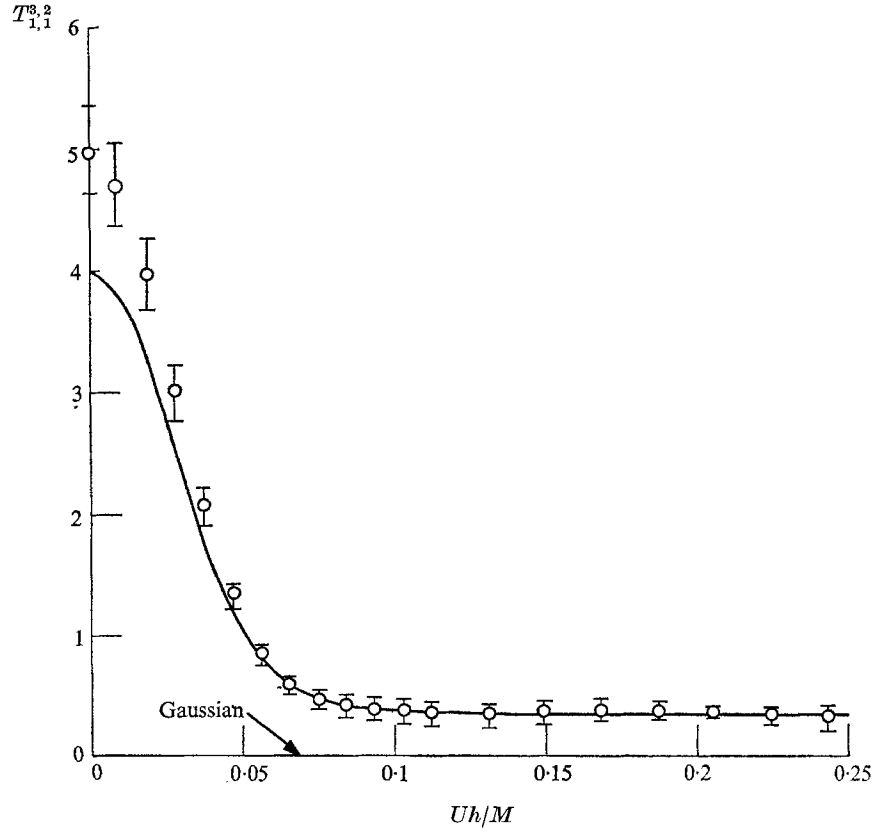


FIGURE 22. Comparison of the measured $T^{3,2}_{1,1}(h)$, at $R_\lambda = 60{\cdot}8$, with the correlation obtained for a fourth-order non-Gaussian probability distribution of $v_t$. ——, fourth-order Gaussian; ○, experimental.

In the case of the fourth-order non-Gaussian probability distribution of $v_t$, equations (14)–(17) yield (for $h = 0$) the following relations between the moments of different orders:

$$\overline{v_t^5}/\overline{v_t^3} = 10, \tag{19}$$

$$\overline{v_t^6}/(\overline{v_t^4} - 2) = 15, \tag{20}$$

$$\overline{v_t^7}/\overline{v_t^3} = 105, \tag{21}$$

$$\overline{v_t^8}/(2\overline{v_t^4} - 5) = 105. \tag{22}$$

It should be noted that except for the ratios of odd-order moments, equations (19) and (21), the above values are the same as for a Gaussian distribution; however, the individual moments $\overline{v_t^n}$ do not have to be Gaussian. Table 3 compares the numerical values given by equations (19)–(22) with those measured at the three turbulence Reynolds numbers.

Similarly, for the sixth-order non-Gaussian probability distribution of $v_t$, the following relations are obtained:

$$\overline{v_t^7}/(\overline{v_t^5} - 5\overline{v_t^3}) = 21, \tag{23}$$

$$\overline{v_t^8}/(4\overline{v_t^6} - 30\overline{v_t^4} + 45) = 7. \tag{24}$$

The ratios in (23) and (24) have the same numerical values for the fourth-order non-Gaussian distribution. However, the sixth-order non-Gaussian distribution does not give the same numerical values for the ratios in (19)–(22).

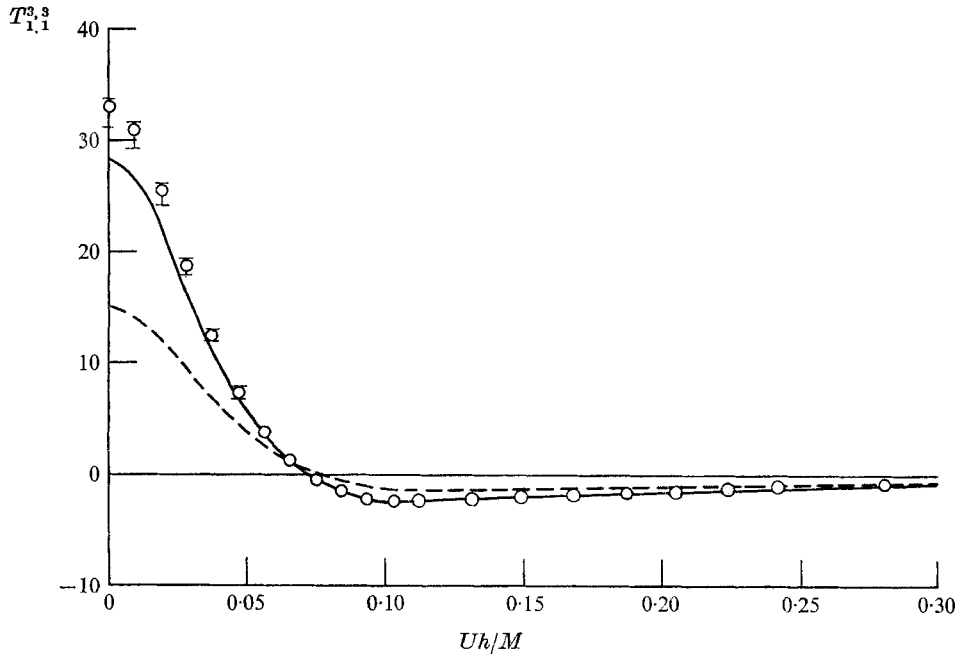


FIGURE 23. Comparison of the measured $T_{1,1}^{3,3}(h)$, at $R_\lambda = 60{\cdot}8$, with the correlations obtained for a Gaussian, and for a fourth-order non-Gaussian probability distribution of $v_t$. – – –, Gaussian; ——, fourth-order non-Gaussian; ○, experimental.

It is of interest to note that, except for the possible effect of frequency response referred to earlier, the trend of the moments in table 2 with Reynolds number is in the opposite direction from that required by various models of the small-scale structure (Corrsin 1962; Tennekes 1968) which require an increasing trend with Reynolds number. Inasmuch as high Reynolds number data over a considerable range are required for proper evaluation, attempts to make such an evaluation have necessarily used available data from a variety of flow configurations (grid turbulence, jet, mixing region, atmospheric turbulence, etc.). However, the possibility does exist that the statistical structure in the various flow configurations may indeed be different. It is therefore desirable that evaluation of this behaviour be carried out for each flow configuration to determine whether such behaviour is universally characteristic for turbulent fields.

It may be noted that the ratios of moments listed in tables 3 and 4 decrease with increasing turbulence Reynolds number. Although it is premature to make any definite conclusions, these ratios indicate an apparent trend toward better agreement with the values given by the non-Gaussian probability distributions at higher Reynolds numbers.

| | $R_\lambda = 37{\cdot}7$ | $R_\lambda = 45{\cdot}2$ | $R_\lambda = 60{\cdot}8$ | Fourth-order non-Gaussian |
|---|---|---|---|---|
| $\overline{v_t^5}/\overline{v_t^3}$ | 14·5 | 13·6 | 12·5 | 10 |
| $\overline{v_t^6}/(\overline{v_t^4}-2)$ | 19·8 | 18·6 | 17·5 | 15 |
| $\overline{v_t^7}/\overline{v_t^3}$ | 291 | 245 | 205 | 105 |
| $\overline{v_t^8}/(2\overline{v_t^4}-5)$ | 258 | 205 | 179 | 105 |

TABLE 3

| | $R_\lambda = 37{\cdot}7$ | $R_\lambda = 45{\cdot}2$ | $R_\lambda = 60{\cdot}8$ | Sixth-order non-Gaussian |
|---|---|---|---|---|
| $\overline{v_t^7}/(\overline{v_t^5}-5\overline{v_t^3})$ | 30·7 | 28·4 | 27·5 | 21 |
| $\overline{v_t^8}/(4\overline{v_t^6}-30\overline{v_t^4}+45)$ | 9·40 | 8·42 | 8·25 | 7 |

TABLE 4

The authors wish to express their gratitude to K. D. Tidstrom and to L. M. Sargent for their assistance in the recording of analog data and the hot-wire instrumentation, and to Mrs Dolores R. Wallace and T. M. Poitras for their aid in connexion with the high-speed computing.

This paper includes the results presented at the Boeing Symposium on Turbulence held in Seattle, Washington 23–27 June 1969. This work was supported in part by the U.S. Atomic Energy Commission.

## REFERENCES

BATCHELOR, G. K. & TOWNSEND, A. A. 1947 *Proc. Roy. Soc.* A **190**, 534.
BATCHELOR, G. K. & TOWNSEND, A. A. 1949 *Proc. Roy. Soc.* A **199**, 238.
CORRSIN, S. 1962 *Phys. Fluids*, **5**, 1301.
FRENKIEL, F. N. & KLEBANOFF, P. S. 1965 *Phys. Fluids*, **8**, 2291.
FRENKIEL, F. N. & KLEBANOFF, P. S. 1967 *a Phys. Fluids*, **10**, 507.
FRENKIEL, F. N. & KLEBANOFF, P. S. 1967*b Phys. Fluids*, **10**, 1737.
GURVICH, A. S. & YAGLOM, A. M. 1967 *Phys. Fluids Suppl.* **10**, S 59.
HELLAND, K. N. & STEGEN, G. R. 1970 *Phys. Fluids*, **13**, 2925.
KAMPÉ DE FÉRIET, J. 1966 *David Taylor Model Basin Report* 2013.
KOLMOGOROFF, A. N. 1962 *J. Fluid Mech.* **13**, 82.
OBUKHOV, A. M. 1962 *J. Geophys. Research*, **67**, 3011; also *J. Fluid Mech.* **13**, 77.
SANDBORN, V. A. 1959 *J. Fluid Mech.* **6**, 221.
STEWART, R. W. & TOWNSEND, A. A. 1951 *Phil. Trans. Roy. Soc.* A**867**, 359.
TENNEKES, H. 1968 *Phys. Fluids*, **11**, 669.
VAN ATTA, C. W. & CHEN, W. Y. 1968 *J. Fluid Mech.* **34**, 497.